Chemical Science

ROYAL SOCIETY OF CHEMISTRY

EDGE ARTICLE

View Article Online
View Journal | View Issue

Cite this: *Chem. Sci.*, 2021, **12**, 11138

All publication charges for this article have been paid for by the Royal Society of Chemistry

Received 20th April 2021
Accepted 7th July 2021

DOI: 10.1039/d1sc02200h

rsc.li/chemical-science

Defining the conditions for the development of the emerging class of Fe^{III}-based MRI contrast agents†

Zsolt Baranyai, [a] Fabio Carniato, [b] Alessandro Nucera,[b] Dávid Horváth, [ac] Lorenzo Tei, [b] Carlos Platas-Iglesias *[d] and Mauro Botta *[b]

Fe(III) complexes are attracting growing interest in chemists developing diagnostic probes for Magnetic Resonance Imaging because they leverage on an endogenous metal and show superior stability. However, in this case a detailed understanding of the relationship between the chemical structure of the complexes, their magnetic, thermodynamic, kinetic and redox properties and the molecular parameters governing the efficacy (relaxivity) is still far from being available. We have carried out an integrated ^{1}H and ^{17}O NMR relaxometric study as a function of temperature and magnetic field, on the aqua ion and three complexes chosen as reference models, together with theoretical calculations, to obtain accurate values of the parameters that control their relaxivity. Moreover, thermodynamic stability and dissociation kinetics of the Fe(III) chelates, measured in association with the ascorbate reduction behaviour, highlight their role and mutual influence in achieving the stability required for use *in vivo*.

1. Introduction

The success and development of MRI as a diagnostic technique of primary importance has been accompanied and facilitated by the availability of metal-based contrast agents (CAs), which allow very important objectives to be achieved: (i) increase the signal intensity; (ii) decrease image acquisition times; (iii) improve image contrast and thus the diagnosis of different malignancies that could remain undetected using unenhanced procedures; (iv) reduce artefacts and improve cost management. The CAs currently used in clinical practice are small and hydrophilic paramagnetic Gd(III) complexes that accelerate the relaxation rates (R_1 and R_2) of proximate tissue water protons in regions of agent accumulation.[1] In addition to these low molecular weight complexes, many other systems, from polynuclear complexes to sophisticated nanosized structures, supramolecular adducts or theranostic agents, have been designed and developed for bio-medical applications and preclinical research.[2]

The success of Gd-based contrast agents (GBCA) was possible thanks to the detailed understanding of the correlation between the efficacy (relaxivity, r_1) and the structural and dynamic parameters that characterize these coordination compounds. In summary, the key parameters are the tumbling rate of the complex in solution ($1/\tau_R$), the exchange rate ($k_{ex} = 1/\tau_M$) of the water molecule in the inner sphere of coordination and its distance (r_{GdH}) from the metal centre, the electronic relaxation times ($T_{1,2e}$) of the paramagnetic ion and its hydration state (q).[1,3] Despite the fact that the clinically used Gd(III) chelates are generally very safe and very well tolerated by patients, there has been recently some concerns related to (i) a new disease, called nephrogenic systemic fibrosis, which was associated with the administration of GBCAs to patients with severely compromised kidney function[4] and (ii) the retention of small amounts of Gd in the tissues of patients exposed to multiple MRI scans, although without any evidence that this is associated with clinical harm.[5] This has given a boost to exploratory research activities focused on finding alternative contrast enhancer based on different chemical species. One obvious and effective approach is the development of contrast agents based on paramagnetic metal ions with improved tolerability. Among them, Mn(II) has received great attention over the past few years, with some of the complexes showing very promising properties.[6] However, while it has been demonstrated that Mn(II)-based MRI probes may have an efficacy quite comparable to that of GBCAs, the challenges remain open in achieving sufficient thermodynamic stability and kinetic inertness for clinical applications.[6] More recent reports have also considered the use of high-spin Fe(III) complexes,[7] which share the same d^5 configuration with the Mn(II)

[a]*Bracco Research Centre, Bracco Imaging S.p.A., Via Ribes 5, 10010, Colleretto Giacosa, Italy*

[b]*Dipartimento di Scienze e Innovazione Tecnologica, Università del Piemonte Orientale "A. Avogadro", Viale T. Michel 11, 15121 Alessandria, Italy. E-mail: mauro.botta@uniupo.it*

[c]*Department of Physical Chemistry, University of Debrecen, Egyetem tér 1., H-4010, Debrecen, Hungary*

[d]*Centro de Investigacións Científicas Avanzadas (CICA), Departamento de Química, Facultade de Ciencias, Universidade da Coruña, 15071 A Coruña, Galicia, Spain. E-mail: carlos.platas.iglesias@udc.es*

† Electronic supplementary information (ESI) available: Experimental details: thermodynamic, kinetic and redox studies. Equations used, NMRD profiles and DFT optimized structures. See DOI: 10.1039/d1sc02200h

analogues, but with a superior safety profile, since iron is an essential element for life present in 3–5 g in the human body.[8] In particular, Schellenberger *et al.*[9] showed that low molecular weight Fe(III) complexes such as $[Fe(CDTA)]^-$ provide significant image contrast *in vivo* and present enhancement kinetics very similar to $Gd(DTPA)^{2-}$, (Magnevist®) a clinically used agent. Subsequently, Gale[10] and Morrow[11] reported Fe(III) complexes with relatively high relaxivities at the imaging fields. Alternatively, Fe(II/III) complexes have been used for redox-dependent paramagnetic chemical exchange saturation transfer (PARACEST) applications or ^{19}F MRI thermometers.[12,13] Overall, these recent results indicate a promising new way to design novel contrast media for MRI, using an endogenous paramagnetic metal alternative to Gd. Despite these important initial contributions, the mechanisms responsible for water proton relaxation enhancement induced by Fe(III) complexes and the relationships between the molecular parameters that govern r_1 and the chemical structure have not been yet deciphered, preventing the development of systems with optimal properties through rational ligand design.

In this paper, we address some basic issues related to the relaxation of the solvent water protons by Fe(III) ions in some model systems, as a necessary initial step towards a detailed evaluation of the efficacy of Fe(III) complexes as diagnostic MRI probes. As stated by S. Koenig over 35 years ago, the Fe(III) ion has the potential to be particularly suitable as an MRI probe due to its relatively large magnetic moment and because it occurs *in vivo* in a variety of forms.[14] Thus, we report here the first detailed ^1H and ^{17}O NMR relaxometric analysis, combined with theoretical calculations of four representative Fe(III) complexes: $Fe(EDTA)^-$, $Fe(CDTA)^-$, $Fe(DTPA)^{2-}$ and the aqua ion $[Fe(H_2O)_6]^{3+}$. In addition, thermodynamic, kinetic and ascorbate reduction studies on $Fe(EDTA)^-$ and $Fe(CDTA)^-$ complexes are reported to assess the overall stability of the complexes (Scheme 1).

2. Results and discussion

The ^1H nuclear magnetic relaxation dispersion (NMRD) profiles recorded for the $[Fe(H_2O)_6]^{3+}$ complex, measured over an extended range of Larmor frequencies, are presented in Fig. 1. Since water exchange is a key dynamic parameter that often affects the relaxivity of metal complexes, we also measured ^{17}O transverse relaxation rates and chemical shifts, which provide direct access to k_{ex}. These data were obtained at low pH (pH = 0–0.5) to avoid the hydrolysis of the cation and formation of hydroxo-species. ^1H NMRD and ^{17}O NMR data were reported several years ago in separate papers.[15,16] These studies provided

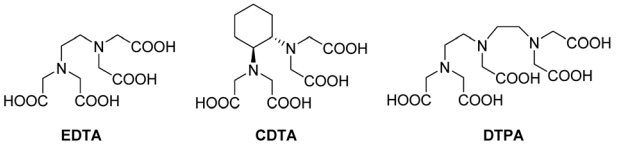

Scheme 1 Ligands discussed in the present work.

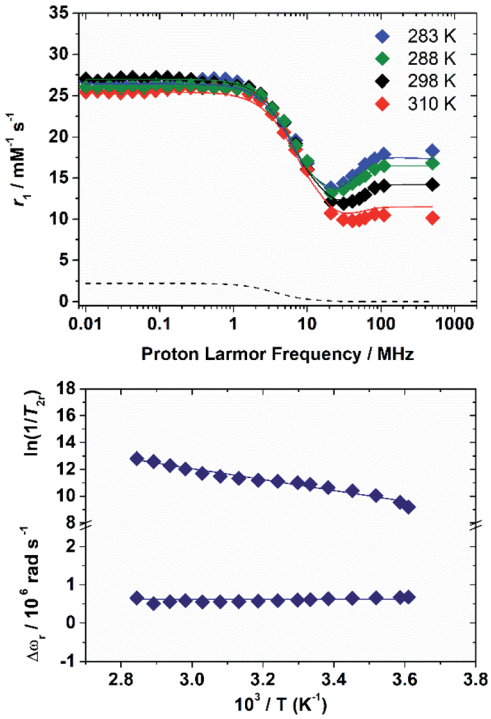

Fig. 1 ^1H NMRD profiles at different temperatures (top) and ^{17}O NMR data (bottom) recorded for $[Fe(H_2O)_6]^{3+}$. The lines correspond to the fits of the data as described in the text. The dashed curve under the NMRD profiles represents the scalar contribution to r_1 at 298 K.

markedly different $^{298}\tau_M$ values of 0.39 μs (^1H NMR) and 14.7 μs and 6.25 ms (^{17}O NMR). The ^1H NMRD profiles show a dispersion in the range 1–20 MHz, as typically observed for low-molecular weight Mn(II) and Gd(III) complexes. The relaxivity of $[Fe(H_2O)_6]^{3+}$ increases above 20 MHz until *ca.* 100 MHz, and then remains fairly constant up to 500 MHz. The ^{17}O transverse relaxation data are characteristic of a system in the slow exchange regime, where T_{2r} increases with increasing temperature.

Initial attempts to fit the ^{17}O NMR and ^1H NMRD data using the same exchange rate failed and provided evidence that proton exchange and the exchange of the whole water molecule occur in different timescales. We therefore carried on a simultaneous fit of the two data sets using the established equations for paramagnetic relaxation[17] and assuming two different residence times: $^{298}\tau_M^H$ (^1H) and $^{298}\tau_M^O$ (whole water). The ^{17}O NMR data were analysed using the Swift–Connick equations,[18] which depend on longitudinal ($i = 1$) and transverse ($i = 2$) relaxation times of the electron spin (T_{ie}) as well as $^{298}\tau_M^O$ and the hyperfine coupling constant $A_O/\hbar$. The whole set of equations used for the analysis of the experimental data is reported in the ESI.† Given the large number of parameters that affect the ^{17}O NMR and NMRD data, we estimated some of them with the use of DFT calculations, while some others were fixed to reasonable values. Following our previous work on Mn(II) complexes,[19] the ^1H and ^{17}O hyperfine coupling constants and the distances between the H atoms of the coordinated water molecules and the paramagnetic centre were estimated from DFT calculations (Table 1).

Table 1 Parameters obtained from the simultaneous fit of ^{1}H NMRD and ^{17}O NMR data[a]

	$[Fe(H_2O)_6]^{3+}$[d]	$Fe(EDTA)^-$	$Fe(CDTA)^-$
$^{298}r_1$ 20 MHz [mM^{-1} s^{-1}]	12.1	2.1	2.4
$^{298}\Delta^2$ [10^{20} s^{-2}]	4.2 ± 0.3	27.0 ± 1.4[e]	18.1 ± 1.3[e]
$^{298}\tau_V$ [ps]	5.3 ± 0.3	2.8 ± 0.1	3.4 ± 0.2
$A_O/\hbar$ [10^6 rad s^{-1}]	−99.3[b,c]	−64.8[b,c]	−62.8[b,c]
$^{298}\tau_M^O$ [ns]	25 000 ± 3600	0.9 ± 0.9	36 ± 4.4
ΔH_M [kJ mol^{-1}]	31.4 ± 4.4	30.5 ± 1.4	51.5 ± 9.9
$^{298}\tau_R$ [ps]	60.7 ± 1.5	35.1 ± 1.7	48.4 ± 2.3
E_R [kJ mol^{-1}]	17.9 ± 1.0	25.2 ± 2.4	21.1 ± 2.3
q	6[b]	1[b]	1[b]
r_{FeH} [Å]	2.69[b,c]	2.69[b,c]	2.70[b,c]
a_{FeH} [Å]	3.5[a]	3.5[a]	3.5[a]

[a] Additional parameters fixed for fitting: $E_V = 1$ kJ mol^{-1}; $^{298}D = 2.24 \times 10^5$ cm^2 s^{-1}; $E_D = 20$ kJ mol^{-1}. [b] Parameters fixed during the fitting procedure. [c] Values obtained with DFT calculations. [d] A scalar contribution to relaxivity was included, with $A_H/\hbar$ fixed to the DFT value of 8.6 × 10^6 rad s^{-1}. An outer-sphere contribution to the chemical shifts with $C_{OS} = 0.038 \pm 0.007$ was considered. Proton exchange is characterized by $^{298}\tau_M^H = 756 \pm 129$ ns and $\Delta H_H^H = 28.2 \pm 4.1$ kJ mol^{-1} in 0.15 M HNO_3 solution. [e] The activation energy for the modulation of the ZFS $E_\Delta = 7.8 \pm 0.5$ and 9.8 ± 0.5 kJ mol^{-1} for $Fe(EDTA)^-$ and $Fe(CDTA)^-$.

These calculations were performed on $[Fe(H_2O)_6]^{3+}\cdot 12H_2O$, which includes 12 explicit second sphere water molecules. The fit of the data required including a scalar contribution to r_1, which depends on the hyperfine coupling constant $A_H/\hbar$. The scalar contribution was found to provide a small, but significant (≈10%), contribution at low fields (<1 MHz).

The residence lifetime of the whole water molecule in the Fe(III) coordination sphere is rather long ($^{298}\tau_M^O = 25$ μs). This can be ascribed to the high charge-to-radius ratio of the cation (*cf.* $^{298}\tau_M^O = 35$ ns for Mn(II)).[20] Water exchange appears to be much faster however than estimated previously by Jordan ($^{298}\tau_M^O = 6.25$ ms).[16] The residence lifetime of water protons obtained from ^{1}H NMRD measurements is much shorter ($^{298}\tau_M^H = 0.76$ μs, Table 1), which indicates that ^{1}H exchange receives an important contribution from prototropic exchange under highly acidic conditions, as recently shown for Gd-complexes bearing amide ancillary groups.[21] Therefore, the observed exchange rate k can be expressed as $k = k_{ex}^{H_2O} + k_H[H^+]$, where $k_{ex}^{H_2O}$ and k_H are the rate constants characterizing the exchange of the whole water molecule and the prototropic mechanism, respectively. Since $k_{ex}^{H_2O} = 4.0 \times 10^4$ s^{-1} and $k_H = 9.06 \times 10^6$ s^{-1} M^{-1}, the prototropic exchange is expected to provide the main contribution at the acidic pH values required to avoid the hydrolysis of $[Fe(H_2O)_6]^{3+}$. These results explain the discrepancies between the data reported earlier on by Merbach and Bertini,[15] and indicate that the $^{298}\tau_M^O$ value calculated by Jordan is very inaccurate. Finally, it is worth noting that the calculated k_H value is 3–4 times larger than that calculated through a pH-dependent study for a cationic GdDOTA-tetraamide derivative.[22]

The inner-sphere contribution to relaxivity is given by eqn (1), where q is the number of coordinated water molecules and T_{1M} is the relaxation time of a coordinated water molecule.

$$r_1^{IS} = \frac{q}{55.55}\frac{1}{T_{1M} + \tau_M} \quad (1)$$

At high magnetic fields (>20 MHz), T_{1M} can be approximated by eqn (2) and (3).

$$\frac{1}{T_{1M}} \cong \frac{2}{15}\gamma_I^2 g_e^2 \mu_B^2 S(S+1) r_{FeH}^{-6}\left[\frac{3\tau_{c1}}{1+\omega_I^2\tau_{c1}^2}\right] \quad (2)$$

$$\frac{1}{\tau_{c1}} = \frac{1}{\tau_M} + \frac{1}{\tau_R} + \frac{1}{T_{1e}} \quad (3)$$

In the case of low molecular weight Mn(II) and Gd(III) complexes τ_M and T_{1e} are generally in the ns timescale, while τ_R is in the ps timescale, so that $\tau_{c1} \cong \tau_R$.[1] For $[Fe(H_2O)_6]^{3+}$ the relaxation of the electron spin is faster and $^{298}\tau_M^H$ is also relatively long, and thus τ_{c1} receives significant contributions from both T_{1e} and τ_R at high magnetic fields, explaining the different shapes of the ^{1}H NMRD profiles of Fe(III), Gd(III) and Mn(II) complexes (Fig. 2). In detail, the NMRD profile simulated for Mn(II) shows a dispersion in the range 0.01 to 0.1 MHz related to the scalar contribution to relaxivity. The relaxivity decreases above 1 MHz, reaching a value of *ca.* 2 mM^{-1} s^{-1} above 100 MHz. The lower relaxivity of Mn(II) at high fields is due to the lower value of $S(S+1)$ compared with Gd(III), an effect partially balanced by a shorter metal–proton distance of the coordinated water molecule (r_{GdH} and r_{MnH} were estimated to be 3.1 and 2.83 Å, respectively).[6] The relaxivity simulated for Fe(III) is relatively low at low fields, as a result of a faster electron relaxation. However, r_1 calculated at high fields is comparable, or higher, to that of Gd(III), which is explained by the contribution of T_{1e} to τ_{c1}, as well as by the short r_{FeH} distance (2.69 Å, as estimated using DFT). From these results we can draw the following important conclusion: small Fe(III) complexes may provide relaxivities quite comparable to those of GBCAs with the same number of coordinated water molecules at the magnetic fields commonly used in MRI.

Once the relaxometric properties of the $[Fe(H_2O)_6]^{3+}$ complex were deciphered, we turned our attention to the complexes with $EDTA^{4-}$ and $CDTA^{4-}$, which are known to contain a water

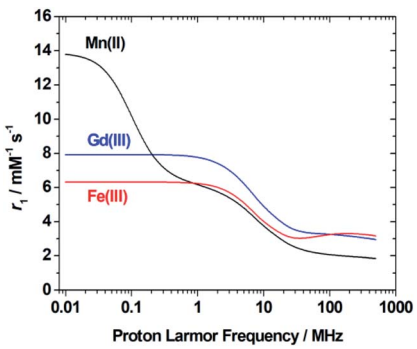

Fig. 2 ^{1}H NMRD profiles simulated for $q = 1$ complexes of Fe(III), Mn(II) and Gd(III) using the parameters determined for the corresponding aqua-ions.

molecule coordinated to the Fe(III) ion.[23] $Fe(EDTA)^-$ represents the prototype and model system of monohydrate iron(III) complexes ($q = 1$), but although some relaxometric data were published in the mid-1980s,[24] a complete and in-depth relaxometric study is yet missing. In particular, it is known that at neutral pH the Fe(III) ion is heptacoordinate with a water molecule in its first coordination sphere characterized by a relatively fast exchange rate. We decided to carry out a complete study of this complex, together with the corresponding iron chelates of DTPA and CDTA, combining ^1H e ^{17}O NMR relaxometric measurements. Both metal chelates have a well-known pH-dependent chemical speciation (Fig. S3 and S4†), which is reflected in the corresponding dependence of r_1 on pH, as shown in Fig. 3. Relaxivity is constant in the acidic zone and up to pH *ca.* 6.5 for $Fe(EDTA)^-$ and 8.5 for $Fe(CDTA)^-$, where deprotonation of the bound water occurs followed by hydrolysis and formation of more complex species.

Therefore, the relaxometric data were measured at pH = 5.3 where only the species $[FeL(H_2O)]^-$ is present in solution. To gain insight into the molecular parameters that control the relaxivity of the Fe(III) species, ^1H $1/T_1$ NMRD profiles were recorded at three different temperatures (283, 298 and 310 K) over a range of magnetic field strengths of 2.3×10^{-4} to 3.0 T, which correspond to proton Larmor frequencies of 0.01–127 MHz (Fig. 4). An additional value at 500 MHz was measured using a high-resolution NMR spectrometer. The profiles of the two complexes reproduce the characteristic properties observed for the aqua ion, *i.e.*: a plateau at low fields, a dispersion around 10 MHz, a minimum around 50–70 MHz followed by a marked increase with the observation frequency to give a large hump centred around 300 MHz. The amplitude of the NMRD profiles (Fig. S11 and S12†) decreases with increasing temperature across the entire range of observed frequencies (0.01–500 MHz). This shows that the residency time of the coordinated water molecule does not influence r_1, which implies that the systems are in the condition of fast exchange. This agrees with the conclusions of a previous ^{17}O NMR study.[25] Thus, the shape of the profiles confirms that, at magnetic field values of clinical MRI relevance, both molecular tumbling and electron relaxation influence relaxivity. The latter increases with the increase of the applied magnetic field and is therefore responsible for the r_1 increase at frequency values greater than 50 MHz. This in an interesting and clearly distinct behaviour from that of the small complexes of Gd(III) and Mn(II).

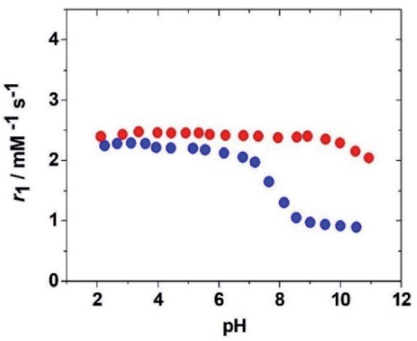

Fig. 3 pH dependency of the relaxivity, r_1, at 298 K and 20 MHz for the complexes $Fe(EDTA)^-$ (blue symbols) and $Fe(CDTA)^-$ (red symbols).

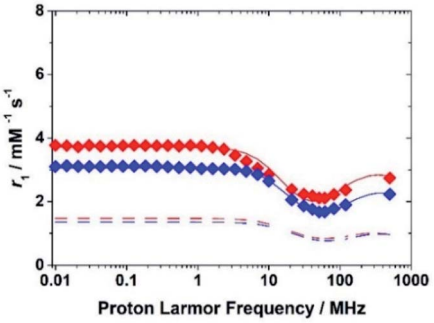

Fig. 4 ^1H NMRD profiles at 298 K for the complexes $Fe(EDTA)^-$ (blue symbols) and $Fe(CDTA)^-$ (red symbols). The lower dashed curves show the calculated outer-sphere contribution.

The effect of molecular tumbling appears to be relevant in explaining the differences in the profiles of the iron complexes with EDTA and CDTA. In fact, while the molecular mass of $Fe(CDTA)^-$ is about 15% greater than that of the EDTA complex, its relaxivity values are about 20–25% higher (at 60 and 120 MHz).

Although there is no clear evidence of an influence of the water exchange rate, k_{ex}, in the NMRD profiles, determining the value of this parameter is very important, as it can become a key factor in the development of neutral complexes or macromolecular systems. An estimate of the k_{ex} values for the two Fe(III) chelates were obtained about twenty years ago by measuring the temperature dependence of the ^{17}O line broadening over a wide temperature range (273 to 388 K).[23]

A more accurate assessment is obtained by measuring the temperature dependence of the solvent ^{17}O NMR transverse relaxation rates, R_2, and shifts, $\Delta\omega$, of concentrated solutions of the complexes and by performing a simultaneous global fit of the ^1H and ^{17}O NMR data.

We collected the data on 4.5 mM solutions of the complexes at pH = 5.5 and 11.75 T (Fig. 5).

The quantitative analysis of the ^1H NMRD and ^{17}O NMR data of $Fe(CDTA)^-$ and $Fe(EDTA)^-$ was performed in a similar way than for $[Fe(H_2O)_6]^{3+}$. The parameters characterizing the outer-sphere contribution (^{298}D, E_D and a_{FeH}) were fixed, while the values of $A_O/\hbar$ and r_{FeH} were estimated with DFT calculations (Table 1). Seven-coordinate complexes with EDTA-like ligands can give rise to two diastereoisomeric forms with capped trigonal prismatic [CTP, $\Delta(\delta)/\Lambda(\lambda)$ enantiomeric pair] and pentagonal bipyramidal [PB, $\Delta(\lambda)/\Lambda(\delta)$ enantiomeric pair] coordination environments.[26] Our calculations show that for $Fe(CDTA)^-$ the CTP geometry is more stable than the PB one by a Gibbs free energy difference of 23.6 kJ mol^{-1}. However, the two diastereoisomers are virtually isoenergetic in the case of $Fe(EDTA)^-$, with the PB isomer being favoured by only 0.1 kJ mol^{-1}. Thus, the CTP diastereoisomer is likely the only one present in solution for $Fe(CDTA)^-$, while in the case of $Fe(EDTA)^-$ both the CTP and PB isomers present significant

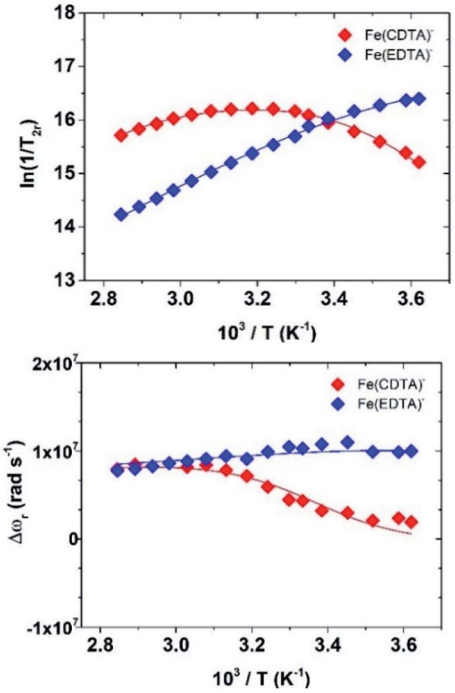

Fig. 5 Temperature dependence of the reduced water ^{17}O NMR transverse relaxation rates (top) and chemical shifts (bottom) for the complexes $Fe(EDTA)^-$ and $Fe(CDTA)^-$. Data measured at 67.78 MHz (11.74 T).

populations in solution. Nevertheless, the two isomers are characterized by similar $A_O/\hbar$ and r_{FeH} values (Table S2†). The analysis of the NMRD data did not require including a scalar contribution to relaxivity, which is likely related to low $A_O/\hbar$ values of the proton nuclei of coordinated water molecules, as suggested by DFT. Finally, the temperature dependence of relaxivity could be well reproduced by allowing the zero-field splitting energy Δ to vary with temperature, following an Arrhenius behaviour with activation energy E_Δ. It is well established that relaxation of the electron spin may be the result of both transient and static ZFS contributions. For highly symmetrical complexes such as $[Fe(H_2O)_6]^{3+}$, the ZFS energy is very small (CASSCF/NEVPT2 calculations based on a CAS(5,5) active space provide $\Delta = 0.036$ cm^{-1}, Table S2†). In this case electron spin relaxation originates from the transient ZFS, which is associated with transient distortions of the metal coordination environment occurring in solution. The static ZFS corresponds to the averaged value of all configurations existing in solution. The values of Δ^2 obtained from the fits of the data correspond to $\Delta = 0.28$ and 0.23 cm^{-1} for $[Fe(EDTA)(H_2O)]^-$ and $[Fe(CDTA)(H_2O)]^-$, respectively. CASSCF/NEVPT2 calculations give very similar Δ values for the two complexes ($\sim$0.13 cm^{-1}). The calculated values are reasonably close to the experimental ones, taking into account that dynamic effects were not considered in this study.

The values of the rotational correlation times $^{298}\tau_R$ are quite consistent with the size of the complexes. The longer $^{298}\tau_R$ value obtained for $[Fe(H_2O)_6]^{3+}$ is probably associated with the presence of a well-defined second coordination sphere promoted by the high positive charge density of the metal ion. Water exchange is several orders of magnitude faster in $Fe(EDTA)^-$ and $Fe(CDTA)^-$ than in the aqua-ion. Water exchange is also considerably faster for $Fe(EDTA)^-$ ($k_{ex}^{298} = 104 \times 10^7$ s^{-1}) than for $Fe(CDTA)^-$ ($k_{ex}^{298} = 2.8 \times 10^7$ s^{-1}). The k_{ex}^{298} value obtained for $Fe(CDTA)^-$ is in reasonably good agreement with previous estimates (1.3–1.7 $\times$ 10^7 s^{-1}), while previous works only based on ^{17}O NMR data reported much lower k_{ex}^{298} values for $Fe(EDTA)^-$ (6.0–7.2 $\times$ 10^7 s^{-1}).[23] The k_{ex}^{298} value determined for $Fe(EDTA)^-$ is endowed with a rather large error, as k_{ex} provides a significant contribution to T_{2r} only at low temperatures. Nevertheless, our combined ^1H and ^{17}O NMR data suggests that previous works underestimated the water exchange rate in $Fe(EDTA)^-$. The lower water exchange rate determined for $Fe(CDTA)^-$ can be attributed to the rigidifying effect of the cyclohexyl backbone, which increases the energy cost required to reach the transition state.[27]

The Fe(III) ion forms with the octadentate ligand DTPA a purely outer sphere (OS) complex ($q = 0$), hence it represents an effective model to compare the measured r_1 values with those calculated for the OS contribution. The NMRD profiles of $[Fe(DTPA)]^{2-}$ were measured in the Larmor frequency range 0.01 to 500 MHz and at temperatures of 283, 298 and 310 K, at neutral pH (Fig. S18†). The experimental and calculated OS profiles are completely similar in shape, while small differences in amplitude are associated with small differences in a_{FeH} and in the parameters of the electron relaxation (Table S3†).

The assessment of the thermodynamic stability and kinetic inertness of the metal-based contrast agents is important to avoid the transmetallation and transchelation reactions with the challenging endogenous components. In particular, Fe(III) complexes can hydrolyse forming hydroxo- and oxo-complexes at high pH values and can be transchelated by transferrins. In fact, transferrins, like serum transferrin (sTf), ovotransferrin (OTf) or lactoferrin (LTf), are strong Fe(III)-binding proteins with one Fe(III)-binding site in each lobe.[28] The human sTf and LTf are known to bind Fe(III) with high affinity ($\log K_{FeTf} = 22.8$, $\log K_{Fe2Tf} = 21.5$), which requires the concomitant binding of a synergistic bicarbonate anion.[29] Since serum transferrin is normally only 30% saturated with Fe(III), it retains a relatively high capacity to compete with Fe(III)-complexes. Thus, we conducted potentiometric titrations to determine the protonation constants of the ligands (Table S1, details in the ESI†), while spectrophotometric experiments were performed to determine the equilibrium constants that describe solution speciation of the Fe(III)–EDTA and Fe(III)–CDTA systems (Fig. S3 and S4†). The stability constants ($I = 0.15$ M $NaNO_3$, Table 2) show that the $Fe(CDTA)^-$ complex is significantly more stable than $Fe(EDTA)^-$. The stability constants are significantly lower than those determined in 0.1 M KNO_3 ($\log K_{FeL} = 29.05$ and 24.95 for $Fe(CDTA)^-$ and $Fe(EDTA)^-$, respectively).[25] This indicates that the Na^+ ion reduces the stability of Fe(III)-complexes due to its interaction with the ligands. The equilibrium constants characterizing the deprotonation of the coordinated water molecule ($\log K_{FeLH-1}$) confirm that the hydrolysis does not occur at physiological pH for $Fe(CDTA)^-$, in perfect agreement with the

Table 2 Equilibrium and rate (k_i) constants, and half-lives ($t_{1/2} = \ln 2/k_d$) characterizing the stability and dissociation reactions of Fe(EDTA)$^-$ and Fe(CDTA)$^-$ complexes (0.15 M $NaNO_3$, 25 °C)[a]

	Fe(EDTA)$^-$	Fe(CDTA)$^-$
$\log K_{FeL}$	22.14(4)	24.36(2)
$\log K_{FeLH-1}$	7.51(1)[b]/7.41(2)[c]	9.50(2)[b]/9.58(4)[c]
k_0 (s^{-1})	$(5 \pm 1) \times 10^{-6}$	$(3.2 \pm 0.5) \times 10^{-7}$
k_{OH} (M^{-1} s^{-1})	1.0 ± 0.2	$(3.6 \pm 0.8) \times 10^{-3}$
k_{OH}^2 (M^{-2} s^{-1})	$(1.4 \pm 0.2) \times 10^3$	1.2 ± 0.1
k_d (s^{-1}) at pH = 7.4	2.9×10^{-6}	2.1×10^{-9}
$t_{1/2}$ (h) at pH = 7.4	66	8.9×10^4
$E_{1/2}$ [mV *vs.* SCE][d]	−132.5	−150.5

[a] The definitions and equations used for the evaluation of the thermodynamic and kinetic data are reported in the ESI. [b] From spectrophotometric titrations. [c] From dissociation experiments. [d] From ref. 25 (E(NHE) = E(SCE) + 0.242 V).

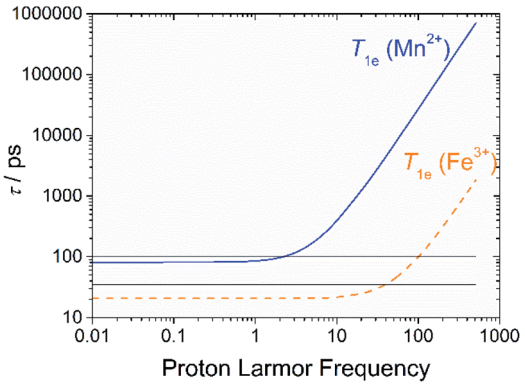

Fig. 6 Values of T_{1e} calculated with the parameters obtained from the relaxometric data of Mn(II) and Fe(III) complexes with EDTA. The horizontal lines indicate the range of τ_R values typical of small complexes (35 to 100 ps).

relaxivity pH dependency showed above. At higher pH, complexes form an oxo-bridged dimer. The equilibrium constants characterizing dimer formation (K_D and K_d, Table S1†) confirm previous results that pointed to a lower tendency of Fe(CDTA)$^-$ to form the oxo-bridged dimer than Fe(EDTA)$^-$.[25]

The kinetic inertness of Fe(EDTA)$^-$ and Fe(CDTA)$^-$ was assessed by transchelation reactions with the HBED ligand, which provided the rates characterizing the spontaneous dissociation k_0 and first- and second-order hydroxide-assisted dissociation rates (k_{OH} and k_{OH}^2, respectively, Table 2).[30] The comparison of the rate constants reported in Table 2 reveals that the spontaneous and the first and second order OH^- assisted dissociations of Fe(EDTA)$^-$ are about 15, 280 and 1200 times faster than those of Fe(CDTA)$^-$. The significantly slower dissociation of the Fe(CDTA)$^-$ is explained by the structural rigidity of the CDTA ligand due to the presence of the cyclohexyl moiety on the ligand backbone,[27] as observed for the Mn(II) analogues.[31] The dissociation rate constant (k_d) of Fe(CDTA)$^-$ calculated near to physiological condition (pH = 7.4, 25 °C), is approximately 1000 times lower than that of Fe(EDTA)$^-$, *i.e.* the former complex is more inert.

It is worth highlighting that for Mn(II) complexes the kinetic inertness is a crucial issue to achieve and typically they follow an acid-assisted dissociation pathway. In general, they tend to form less stable and inert complexes than Fe(III) ($\log K_{MnEDTA}$ = 12.46; $\log K_{MnCDTA}$ = 14.32; $t_{1/2MnEDTA}$ = 0.076 h; $t_{1/2MnCDTA}$ = 12.3 h (pH 7.4)).[31]

Importantly, Fe^{III}-based compounds may participate in the redox cycle by taking the electron from the reducing agent, which is followed by its reduction and the concomitant electron transfer to H_2O_2 (Fenton reaction). According to the concentration and the redox properties of the possible reducing agents in human blood plasma, ascorbic acid is the most relevant candidate to involve Fe^{III}-complexes into the Fenton reaction.[32] The redox stability of Fe(EDTA)$^-$ and Fe(CDTA)$^-$ was investigated *via* the reduction of the Fe^{III}-complexes with ascorbic acid monitored by spectrophotometry (pH = 7.4, 25 °C in 0.15 M $NaNO_3$).

According to the kinetic data, the electron-transfer occurs by the formation of the ternary Fe^{III}L–HA intermediate between the ascorbate anion (HA^-) and the Fe^{III}L complex, likely through the substitution of the inner-sphere water molecule. The formation of a similar ternary Fe(EDTA)–oxalate complex was identified by the pH-potentiometric studies of the Fe(EDTA)–oxalate system (Fe^{III}(EDTA)–Ox: K_{FeL-Ox} = 275 M^{-1}).[33] The k_{HA} rate constants characterizing the ascorbate anion assisted reduction of Fe(EDTA)$^-$ and Fe(CDTA)$^-$ were found to be 8 ± 2 and 3.0 ± 0.2 M^{-1} s^{-1} at pH = 7.4. By taking into account the stability of the ternary Fe^{III}L–HA intermediates (Fe^{III}(EDTA)–HA^-: K_{FeL-HA} = 75 ± 15 M^{-1}; Fe^{III}(CDTA)–HA^-: K_{FeL-HA} = 40 ± 5 M^{-1}) and the *in vivo* concentration of the ascorbate anion ([(HA^-)] = 43 μM),[34] the ascorbate-assisted reduction rate (k_{obs}) and half-lives ($t_{1/2} = \ln 2/k_{obs}$) of Fe(EDTA)$^-$ and Fe(CDTA)$^-$ are 2.4×10^{-4} and 1.3×10^{-4} s^{-1}, (0.8 and 1.5 hours, respectively). Thus, the half-lives of the complexes near physiological condition are about 83 (Fe(EDTA)$^-$) and 59 000 (Fe(CDTA)$^-$) times faster upon reduction than in the absence of the reducing agent.

Based on previous studies[35,36] the ascorbate-assisted reduction rate constant of Fe^{III}L complexes is expected to decrease with the electrode potential of Fe^{III}L, as confirmed by the 1.8 times slower reduction of Fe(CDTA)$^-$ with respect to Fe(EDTA)$^-$. Since the electrode potential is correlated to the thermodynamic stability constant of Fe^{III}L, we emphasize that the thermodynamic properties of the Fe^{III}-complexes play a very important role together to the kinetic ones for their *in vivo* applications. Ascorbic acid is a strong reducing agent ($H_2A \rightarrow A + 2H^+ + 2e^-$ E^0 = 0.39 V *vs.* NHE),[37] however, the reduction potential is strongly influenced by the pH and the formation of the $HA^\bullet$ and $A^{\bullet-}$ radicals as intermediates. Thus, at physiological condition, the electrode potential of the Fe^{III}/Fe^{II}-complex redox couple should be lower than −0.2 V *vs.* NHE to avoid the formation of Fe^{II}-complexes and the occurrence of the Fenton reactions.[37]

3. Conclusions

We have shown here that monohydrated Fe(III) complexes are very attractive candidates for the design of efficient MRI

contrast agents, in particular at the high magnetic fields of modern clinical scanners and of those used in animal studies. The detailed multinuclear relaxometric analysis over a wide range of proton Larmor frequencies, performed for the first time for Fe(III) complexes, revealed some key differences as compared to related Mn(II) and Gd(III) complexes. The relaxivity of Fe(III) complexes at high fields receives contributions from both τ_R and T_{1e}, which assume values of the same order of magnitude between *ca.* 1.5 and 3 T (Fig. 6). On the other hand, T_{1e} is considerably longer for Mn(II) and Gd(III) complexes, hence T_{1e} affects relaxivity only below ~10 MHz. We anticipate that optimization of both T_{1e} and τ_R will allow obtaining Fe(III) complexes with effectiveness (relaxivity) even higher than that of the commercially available and clinically used agents.

Another important conclusion of the present work is that the properties of Fe(III) contrast agent candidates must be tuned to: (i) increase the pK_a of the coordinated water molecule well above physiological pH, (ii) obtain kinetically inert complexes, for example by ligand rigidification, and (iii) shift the reduction potential of the complex out of the biological window (E^0 < −0.2 V *vs.* NHE), to avoid complex dissociation upon reduction and also triggering the Fenton reaction.

In this perspective, coordination chemistry appears to be able to play an important role as two structurally very similar compounds such as the iron(III) complexes of EDTA and CDTA have markedly different pK_a values of bound water. The small structural differences between the two chelates also result in significantly different k_{ex} values and suggests the possibility of modulating this parameter through a suitable chemical design, as successfully happened in the case of Gd(III) complexes. Even the kinetic inertia seems significantly depend on structural aspects seemingly minor. Then, the CDTA scaffold is clearly better suited for the design of Fe(III)-based MRI contrast agents than it is EDTA.

It will be necessary to understand, at least from an empirical point of view through the collection of a large number of new data, if it is conceivable to optimize the electronic relaxation time with an appropriate design of the ligand as this would allow to increase the relaxation and tune the frequency value corresponding at its maximum value. So, while much remains to be done, we hope that these results may represent useful guidelines for the development of metal-diagnostic probes of improved safety, biotolerability and efficacy.

Data availability

The datasets supporting this article have been uploaded as part of the ESI.

Author contributions

CPI and MB conceived and supervised the project. AN carried out the relaxometric study with the assistance of FC and LT. DH and ZB carried out the thermodynamic and kinetic experiments. CPI, AN and MB analysed the relaxometric data. CPI performed the computational study. ZB, LT, CPI and MB wrote the manuscript.

Conflicts of interest

There are no conflicts to declare.

Acknowledgements

F. C., L. T. and M. B. acknowledge the financial support from Università del Piemonte Orientale (Ricerca locale FAR2019). C.P.-I. thanks Ministerio de Economía y Competitividad (CTQ2016-76756-P) and Xunta de Galicia (ED431B 2020/52) for generous financial support. C.P.-I. also thanks Centro de Supercomputación de Galicia (CESGA) for providing the computer facilities. Z. B. thanks the Doctoral School of Chemistry of the University of Debrecen for the PhD position of D. H. This work was carried out within the framework of the COST CA15209 Action "European Network on NMR Relaxometry".

Notes and references

1 (*a*) A. E. Merbach, L. Helm and E. Toth, *The Chemistry of Contrast Agents in Medical Magnetic Resonance Imaging*, John Wiley & Sons Ltd, 2nd edn, 2013; (*b*) J. Wahsner, E. M. Gale, A. Rodríguez-Rodríguez and P. Caravan, *Chem. Rev.*, 2019, **119**, 957–1057.

2 (*a*) E. A. Akam, E. Abston, N. J. Rotile, H. R. Slattery, I. Y. Zhou, M. Lanuti and P. Caravan, *Chem. Sci.*, 2020, **11**, 224–231; (*b*) M. Botta and L. Tei, *Eur. J. Inorg. Chem.*, 2012, 1945–1960; (*c*) A. J. L. Villaraza, A. Bumb and M. W. Brechbiel, *Chem. Rev.*, 2010, **110**, 2921–2959; (*d*) M. C. Heffern, L. M. Matosziuk and T. J. Meade, *Chem. Rev.*, 2014, **114**, 4496–4539; (*e*) E. Di Gregorio, L. Lattuada, A. Maiocchi, S. Aime, G. Ferrauto and E. Gianolio, *Chem. Sci.*, 2021, **12**, 1368–1377; (*f*) C. J. Adams and T. J. Meade, *Chem. Sci.*, 2020, **11**, 2524–2530.

3 S. Aime, M. Botta, D. Esteban-Gómez and C. Platas-Iglesias, *Mol. Phys.*, 2019, **117**, 898–909.

4 (*a*) J. M. Hazelton, M. K. Chiu and H. H. Abujudeh, *Curr. Radiol. Rep.*, 2019, **7**, 5; (*b*) J. Endrikat, S. Dohanish, N. Schleyer, S. Schwenke, S. Agarwal and T. Balzer, *Invest. Radiol.*, 2018, **53**, 541–550.

5 (*a*) E. Gianolio, E. Di Gregorio and S. Aime, *Eur. J. Inorg. Chem.*, 2019, 137–151; (*b*) M. Le Fur and P. Caravan, *Metallomics*, 2019, **11**, 240–254.

6 M. Botta, F. Carniato, D. Esteban-Gomez, C. Platas-Iglesias and L. Tei, *Future Med. Chem.*, 2019, **11**, 1461–1483.

7 (*a*) N. Kuznik and M. Wyskocka, *Eur. J. Inorg. Chem.*, 2015, 445–458; (*b*) M. F. Tweedle, *Radiology*, 2018, **286**, 409–411.

8 G. J Anderson and D. M. Frazer, *Am. J. Clin. Nutr.*, 2017, **106**, 1559S–1566S.

9 (*a*) P. Boehm-Sturm, A. Haeckel, R. Hauptmann, S. Mueller, C. K. Kuhl and E. Schellenberger, *Radiology*, 2018, **286**, 537–546; (*b*) J. Xie, A. Haeckel, R. Hauptmann, I. P. Ray, C. Limberg, N. Kulak, B. Hamm and E. Schellenberger, *Magn. Res. Med.*, 2021, **85**, 3370–3382.

10 H. Wang, V. Clavijo Jordan, I. A. Ramsay, M. Sojoodi, B. C. Fuchs, K. K. Tanabe, P. Caravan and E. M. Gale, *J. Am. Chem. Soc.*, 2019, **141**, 5916–5925.

11 (*a*) E. M. Snyder, D. Asik, S. M. Abozeid, A. Burgio, G. Bateman, S. G. Turowski, J. A. Spernyak and J. R. Morrow, *Angew. Chem., Int. Ed.*, 2020, **59**, 2414–2419; (*b*) D. Asik, R. Smolinski, S. M. Abozeid, T. B. Mitchell, S. G. Turowski, J. A. Spernyak and J. R. Morrow, *Molecules*, 2020, **25**, 2291; (*c*) A. Patel, D. Asik, E. M. Snyder, A. E. Dilillo, P. J. Cullen and J. R. Morrow, *ChemMedChem*, 2020, **15**, 1050–1057.

12 (*a*) S. J. Dorazio and J. R. Morrow, *Eur. J. Inorg. Chem.*, 2012, 2006–2014; (*b*) K. Du, E. A. Waters and T. D. Harris, *Chem. Sci.*, 2017, **8**, 4424–4430; (*c*) I.-R. Jeon, J. G. Park, C. R. Haney and T. D. Harris, *Chem. Sci.*, 2014, **5**, 2461–2465.

13 A. E. Thorarinsdottir, A. I. Gaudette and T. D. Harris, *Chem. Sci.*, 2017, **8**, 2448–2456.

14 S. H. Koenig, C. M. Baglin and R. D. Brown III, *Magn. Reson. Med.*, 1985, **2**, 283–288.

15 (*a*) T. W. Swaddle and A. E. Merbach, *Inorg. Chem.*, 1981, **20**, 4212–4216; (*b*) I. Bertini, F. Capozzi, C. Luchinat and Z. Xia, *J. Phys. Chem.*, 1993, **97**, 1134–1137.

16 M. Grant and R. B. Jordan, *Inorg. Chem.*, 1981, **20**, 55–60.

17 (*a*) I. Solomon, *Phys. Rev.*, 1955, **99**, 559–565; (*b*) N. Bloembergen and L. O. Morgan, *J. Chem. Phys.*, 1961, **34**, 842–850; (*c*) J. H. Freed, *J. Chem. Phys.*, 1978, **68**, 4034–4037.

18 T. J. Swift and R. E. Connick, *J. Chem. Phys.*, 1962, **37**, 307–312.

19 G. A. Rolla, C. Platas-Iglesias, M. Botta, L. Tei and L. Helm, *Inorg. Chem.*, 2013, **52**, 3268–3279.

20 D. Esteban-Gómez, C. Cassino, M. Botta and C. Platas-Iglesias, *RSC Adv.*, 2014, **4**, 7094–7103.

21 L. Leone, M. Boccalon, G. Ferrauto, I. Fabian, Z. Baranyai and L. Tei, *Chem. Sci.*, 2020, **11**, 7829–7835.

22 S. Aime, A. Barge, M. Botta, D. Parker and A. S. De Sousa, *J. Am. Chem. Soc.*, 1997, **119**, 4767–4768.

23 T. Schneppensieper, S. Seibig, A. Zahl, P. Tregloan and R. van Eldik, *Inorg. Chem.*, 2001, **40**, 3670–3676.

24 J. Bloch and G. Navon, *J. Inorg. Nucl. Chem.*, 1980, **42**, 693–699.

25 A. Brausam, J. Maigut, R. Meier, P. A. Szilágyi, H.-J. Buschmann, W. Massa, Z. Homonnay and R. van Eldik, *Inorg. Chem.*, 2009, **48**, 7864–7884.

26 J. Maigut, R. Meier, A. Zahl and R. van Eldik, *Inorg. Chem.*, 2008, **47**, 5702–5719.

27 (*a*) E. Balogh, M. Mato-Iglesias, C. Platas-Iglesias, E. Tóth, K. Djanashvili, J. A. Peters, A. de Blas and T. Rodríguez-Blas, *Inorg. Chem.*, 2006, **45**, 8719–8728; (*b*) G. Tircsó, M. Regueiro-Figueroa, V. Nagy, Z. Garda, T. Garai, F. K. Kalman, D. Esteban-Gómez, E. Tóth and C. Platas-Iglesias, *Chem.–Eur. J.*, 2016, **22**, 896–901.

28 Y. Li, B. Liu, Z. Ge and B. Yang, *J. Photochem. Photobiol., B*, 2008, **91**, 137–142.

29 W. R. Harris and V. L. Pecoraro, *Biochemistry*, 1983, **22**, 292–299.

30 A. Vágner, A. Forgács, E. Brücher, I. Tóth, A. Maiocchi, A. Wurzer, H.-J. Wester, J. Notni and Z. Baranyai, *Front. Chem.*, 2018, **6**, 170.

31 (*a*) F. K. Kalman and G. Tircso, *Inorg. Chem.*, 2012, **51**, 10065–10067; (*b*) K. Pota, Z. Garda, F. K. Kalman, J. L. Barriada, D. Esteban-Gomez, C. Platas-Iglesias, I. Toth, E. Brucher and G. Tircso, *New J. Chem.*, 2018, **42**, 8001–8011.

32 (*a*) W. H. Koppenol and R. H. Hider, *Free Radicals Biol. Med.*, 2019, **133**, 3–10; (*b*) Y. Turyan and R. Kohen, *J. Electroanal. Chem.*, 1995, **380**, 273–277.

33 D. Pyreu and E. Kozlovskii, *Zh. Neorg. Khim.*, 2000, **45**, 459–464.

34 P. M. May, P. W. Linder and D. R. Williams, *J. Chem. Soc., Dalton Trans.*, 1977, 588–595.

35 M. Taqui-Khan and A. E. Martell, *J. Am. Chem. Soc.*, 1968, **90**, 3386–3389.

36 (*a*) E. Pelizzetti, E. Mentasti and E. Pramauro, *Inorg. Chem.*, 1976, **15**, 2898–2900; (*b*) E. Pelizzetti, E. Mentasti and E. Pramauro, *Inorg. Chem.*, 1978, **17**, 1181–1186.

37 J. C. Joyner, J. Reichfield and J. A. Cowan, *J. Am. Chem. Soc.*, 2011, **133**, 15613–15626.